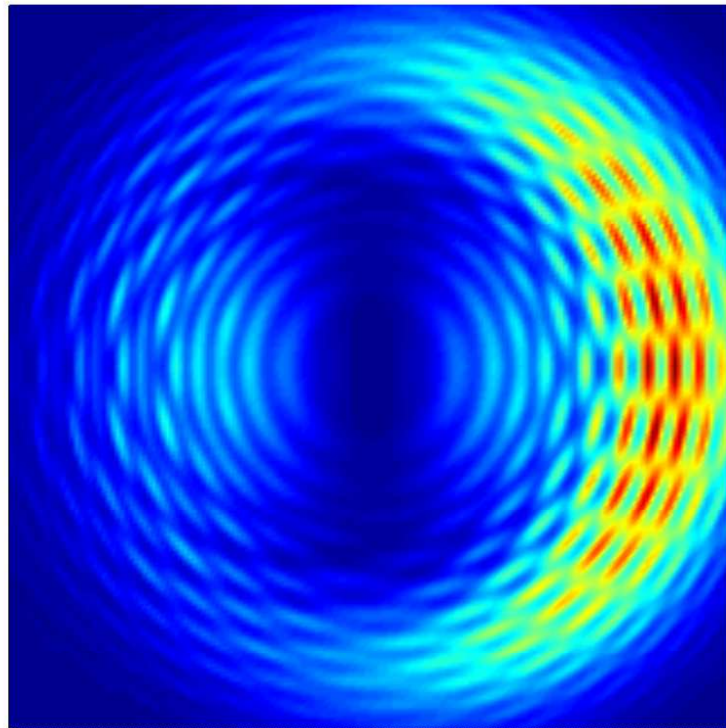


Strong-field ionization of atoms and molecules by few-cycle laser pulses



Christian Per Juul Martiny

Department of Physics and Astronomy
University of Aarhus, Denmark

Progress report
May 2008

Contents

Introduction	1
1 General theory	2
1.1 Light-matter interaction	2
1.2 Few-cycle laser pulses	4
1.3 The strong-field approximation for ionization	5
1.4 The saddle-point method	7
2 Numerical and analytical results	11
2.1 Symmetry of carrier-envelope phase difference effects	11
2.2 Momentum distributions	14
2.2.1 The circular case	14
2.2.2 General Polarization	16
2.3 Angular distributions from laser-aligned CS ₂ molecules: Comparing theory with experiment	20
3 Conclusion and outlook	25
3.1 Conclusion	25
3.2 Outlook	25

Preface

This progress report contains a summary of the work carried out during part A of my PhD study at the Lundbeck Foundation Theoretical Center for Quantum System Research, Department of Physics and Astronomy, University of Aarhus. The main part of the report is based on work described in the four papers [1, 2, 3, 4] regarding strong-field ionization of atoms and molecules by few-cycle laser pulses. The first part of the report contains the necessary theory, while the second part describes the numerical and analytical results obtained during my part A.

Atomic units $m_e = e = \hbar = 1$ are used throughout this report, unless otherwise stated.

Acknowledgements

I would like to thank my supervisor Lars Bojer Madsen for presenting this topic to me and for excellent supervision during part A. In addition, I would like to thank Niels Martiny and Maj-Britt Suhr Kirketerp for proofreading this manuscript.

Introduction

There has been a tremendous development in pulsed laser source technology during the last few years. Pulses with a duration of only a few femtoseconds and intensities comparable to the Coulomb interaction between the electron and the nuclei ($I = 1.0 \times 10^{13} \text{ W/cm}^2$ - $I = 1.0 \times 10^{15} \text{ W/cm}^2$) are now available for wavelengths in the range from 400 nm to 2000 nm [5]. This development has paved the way for exciting new research fields such as attoscience and femtochemistry.

The characteristic timescale for chemical reactions and nuclear motion in diatomic molecules is femtoseconds. It is therefore possible to investigate chemical reactions [6], and nuclear motion [7] in real time, using femtosecond pulses.

The typical timescale for electron dynamics in an atom or molecule is the attosecond, thus preventing electron dynamics from being studied using femtosecond pulses. It is, however, possible to generate XUV attosecond pulses using femtosecond pulses [5]. Attosecond pulses are short enough to capture electron dynamics within an atom, i.e., study the movement of a bound electron.

Consider an atom ionized by a femtosecond pulse. The ejected electron is shaken back and forth by the field, which can drive the electron back towards the residual atom. If the electron recombines with the residual atom, the excess energy will be ejected in one photon with a frequency of $N\omega$, where ω is the laser frequency and N is an integer. This is the process used to generate coherent attosecond pulses. It is called high-harmonic generation (HHG). High-harmonic generation is furthermore used in molecular-orbital tomography, where the goal is to reconstruct the molecular orbital using the HHG-spectrum [8].

In strong-field physics single ionization stands out as a fundamental process since it triggers the subsequent electron wave packet dynamic in the continuum, and hence affects important processes such as HHG. A theoretical description of HHG, requires a description of the first step in HHG, namely the ionization step.

Ionization is furthermore an important ingredient in coherent control with few-cycle pulses, where one of the goals is to be able to control the electron in the continuum and thereby steer reactions [9].

A prerequisite for subsequent steering and manipulation of an electron wave packet is the knowledge of the conditions for the electron just born in the continuum. Confinement in the direction of electron ejection and locality in time depends highly on the exact shape of the pulse and on the pulse length. This dependence is precisely the topic of this part A report.

Chapter 1

General theory

1.1 Light-matter interaction

Consider an atom or molecule interacting with a laser field described by the vector potential $\vec{A}(\vec{r}, t)$ and the scalar potential $V(\vec{r}, t)$. The real physical fields \vec{E} and \vec{B} are obtained from the potentials by $\vec{E} = -\nabla V - \frac{\partial \vec{A}}{\partial t}$ and $\vec{B} = \nabla \times \vec{A}$ [10].

We are going to use a semi-classical approach, where the atomic or molecular system is treated quantum mechanically, while the laser field is treated classically. This is a good approximation in strong-fields, where the number of photons can be approximated by a continuous variable, thus making the field classical. We furthermore neglect the influence of the atom or molecule on the laser field.

In addition we are going to use the single active electron approximation (SAE) throughout the report¹, where we assume that only one electron couples to the field, the rest being frozen out. Consider, for instance a CS₂ molecule. The binding energy of the HOMO electron is 10.08 eV, while the binding energy of the second highest occupied orbital is 14.6 eV. This leads to a strongly suppressed ionization probability of this orbital compared to that of the HOMO, making the SAE a very good approximation. Notice, however, that most of the numerical calculations in this report are performed on hydrogen, where the SAE, of course, is not an approximation.

Now the Hamilton operator H for an electron in an electromagnetic field is [11],

$$H = -\frac{1}{2}\nabla^2 + \vec{A}(\vec{r}, t) \cdot \hat{p} + \frac{1}{2}\vec{A}(\vec{r}, t)^2 \quad (1.1)$$

if we adopt the Coulomb gauge $\nabla \cdot \vec{A} = 0$ and $V = 0$. The time-dependent Schrödinger equation (TDSE) then reads,

$$i\frac{\partial}{\partial t}\Psi(\vec{r}, t) = \left(-\frac{1}{2}\nabla^2 + \vec{A}(\vec{r}, t) \cdot \hat{p} + \frac{1}{2}\vec{A}(\vec{r}, t)^2 + V_B(\vec{r})\right)\Psi(\vec{r}, t) \quad (1.2)$$

where V_B is the atomic or molecular binding potential. The term $\vec{A}(\vec{r}, t) \cdot \hat{p}$ describes the interaction between the active electron and the field, while $\frac{1}{2}\vec{A}(\vec{r}, t)^2$ is

¹except in sec. 2.1

the energy associated with the field itself.

Atoms and (small) molecules extend typically over distances of the order 1 Ångström (10^{-10}m), i.e., their wave functions extend over this distance. The wavelength of the light we are going to consider is, however, of the order 1000 Ångström (100 nm) thousand times larger than the typical atomic distance. This implies that the light field practically does not change over the spatial region of the atom or molecule, so we can neglect the spatial dependence of the fields $\vec{A}(\vec{r}, t) = \vec{A}(t)$. This is the so called dipole approximation, which holds as long as $\lambda \gg a$, with λ being the wavelength, and a a measure of the linear extend of the wave function. Notice, that the B-field component of the electromagnetic field vanishes in the dipole approximation, since $\vec{B} = \nabla \times \vec{A}$. The field energy term $\vec{A}(t)^2$ can be eliminated by the gauge transformation $\exp(i \int^t A^2(t') dt')$ in the dipole approximation [11]. Thus,

$$i \frac{\partial}{\partial t} \Psi(\vec{r}, t) = (H_0 + \vec{A}(t) \cdot \hat{p}) \Psi(\vec{r}, t) \quad (1.3)$$

where H_0 is the field-free Hamiltonian. This description is said to be in the velocity gauge, since the field couples to the velocity. An alternative description is the length gauge, where the electric field couples to the position operator [11]. The TDSE in length gauge is,

$$i \frac{\partial}{\partial t} \Psi(\vec{r}, t) = (H_0 + \vec{E}(t) \cdot \vec{r}) \Psi(\vec{r}, t) \quad (1.4)$$

which is obtained from (1.3) when performing a new gauge transformation $\exp(i \vec{A} \cdot \vec{r})$. Quantum mechanics is gauge-invariant [12], so the two descriptions are completely equivalent. When approximations are evoked, however, gauge invariance is broken and the two different gauges may give different results [13, 14]. The interaction operator in length gauge is proportional to the position vector, which means that length gauge favors large distances in space. Velocity gauge on the other hand favors the part of space where the wave function varies significant, i.e., small distances. We will expect large distances to be the most important part of space in ionization, favoring length gauge as the right description when approximations are used [13, 14]. We will only consider length gauge in this report.

Let us conclude the section by a few remarks regarding the wave function for an electron in an electromagnetic field, the so called Volkov wave function [15, 16]. The TDSE for an electron in an electric field reads,

$$i \frac{\partial}{\partial t} \Psi_{\text{Volkov}}(\vec{r}, t) = \left(\frac{\hat{p}^2}{2} + \vec{E}(t) \cdot \vec{r} \right) \Psi_{\text{Volkov}}(\vec{r}, t) \quad (1.5)$$

in length gauge. It is easily verified by differentiation that the solution, the Volkov wave function, is given by,

$$\Psi_{\text{Volkov}}(\vec{r}, t) = \frac{1}{(\sqrt{2\pi})^3} \exp \left(i(\vec{q} + \vec{A}(t)) \cdot \vec{r} - \frac{i}{2} \int_0^t (\vec{q} + \vec{A}(t'))^2 dt' \right) \quad (1.6)$$

where \vec{q} is the canonical momentum. The Volkov wave is simply a plane wave, with the momentum \vec{q}' given by the kinematical momentum $\vec{q} + \vec{A}$ due to the presents of the field.

1.2 Few-cycle laser pulses

The classical electromagnetic field for an elliptically polarized single mode laser of angular frequency ω propagating in the z -direction is described by the vector potential [17],

$$\vec{A}(t) = A_0 \left(\cos(\omega t + \phi) \cos\left(\frac{\epsilon}{2}\right) \vec{e}_x + \sin(\omega t + \phi) \sin\left(\frac{\epsilon}{2}\right) \vec{e}_y \right) \quad (1.7)$$

in the dipole approximation. Here A_0 is the amplitude, ϕ is a phase, and ϵ is the ellipticity describing all degrees of elliptical polarization when varied within the interval $[0; \frac{\pi}{2}]^2$.

The amplitude A_0 is related to the electric field amplitude by $E_0 = \omega A_0$, and the relation to the intensity is $I = E_0^2$, which is obtained by looking at the Poynting vector [10]. All physical processes induced by a field like (1.7), with infinite temporal extension, is of course independent of ϕ but ϕ is, as we shall see shortly, a very important quantity for few-cycle pulses. A field like (1.7) with infinite temporal extension cannot describe a few-cycle pulse, i.e., a pulse with a finite duration. Such a pulse can be produced by a superposition of plane waves (1.7) with different frequencies. A popular form for the vector potential describing a few-cycle pulse is,

$$\vec{A}(t) = A_0 f(t) \left(\cos(\omega t + \phi) \cos\left(\frac{\epsilon}{2}\right) \vec{e}_x + \sin(\omega t + \phi) \sin\left(\frac{\epsilon}{2}\right) \vec{e}_y \right) \quad (1.8)$$

where f is the envelope which is zero everywhere, except in the interval $t \in [0; \tau]$ where τ is the pulse duration. The envelope f is a slowly varying function compared to the carrier wave $(\cos(\omega t + \phi) \cos(\frac{\epsilon}{2}) \vec{e}_x + \sin(\omega t + \phi) \sin(\frac{\epsilon}{2}) \vec{e}_y)$. We will use $f(t) = \sin^2\left(\frac{\omega t}{2N}\right)$, where N is the number of optical cycles. Other forms of envelopes are square-, trapezoidal, and gaussian-envelopes. The quantity ω is called the central frequency, and it is (close to) the most dominant frequency among the frequencies of which the pulse is composed. The electric field $\vec{E}(t) = -\frac{\partial}{\partial t} \vec{A}(t)$ originating from (1.8) depends highly on the phase ϕ , as shown in fig. 1.1. A few-cycle pulse is general quite asymmetric in space, and the phase ϕ determines this asymmetry. It is called the carrier-envelope phase difference (CEPD), since it gives the phase difference between the carrier wave and the envelope in the linear case. Notice, that the electric field in the circular case rotates around the z axis by an angle $\Delta\phi$ when the CEPD is change by $\Delta\phi$. We will return to this point in sec. 2.1, where we fully characterizes the response of atomic and molecular systems under a change of the CEPD.

The electric field originating from (1.8) satisfies the relation $\int_0^\tau \vec{E} dt = \vec{0}$. A physical

² $\epsilon = 0$ corresponds to linear polarization, while $\epsilon = \frac{\pi}{2}$ corresponds to circular.

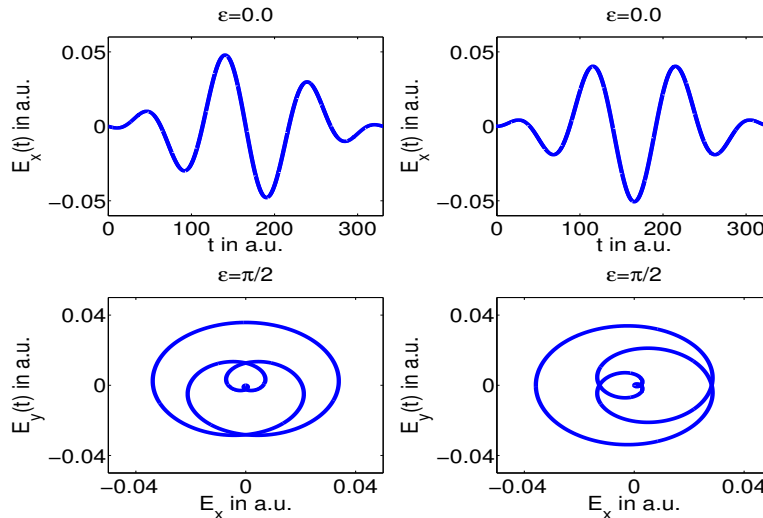


Figure 1.1: The electric field obtained from (1.8) for two different polarizations and two different values of CEPD. The upper row shows the electric field in the case of linear polarization for $\phi = 0$ (left), and $\phi = \frac{\pi}{2}$ (right). The lower row shows the electric field in the case of circular polarization for $\phi = 0$ (left), and $\phi = \frac{\pi}{2}$ (right). The parameters are $I = 9.0 \times 10^{13} \text{ W/cm}^2$, $\omega = 0.057$ corresponding to a central wavelength of 800nm and three cycles, $N = 3$.

pulse has to obey this relation, since it otherwise would contain a DC component ($\vec{E}(\omega = 0) = \int_0^\tau \vec{E} dt$), which is, of course, not possible for a propagating pulse.

1.3 The strong-field approximation for ionization

Having presented the general setup, we are now ready to present an approximate method of calculating the transition amplitude for direct ionization of an atom or molecule by an external electric field. The approximation called the strong-field approximation (SFA) [18, 19, 20, 21], is based on a S-matrix expansion and is widely used within the field [22].

Consider an atom or a molecule, initially in its ground state, interacting with an external time-dependent potential $V(t)$, e.g., $V(t) = \vec{r} \cdot \vec{E}(t)$ in length gauge. The time-dependent Schrödinger equation reads,

$$i \frac{\partial}{\partial t} \Psi = (H_0 + V(t)) \Psi \quad (1.9)$$

where H_0 is the field-free Hamiltonian. It is not possible to solve this equation analytically, so we have two options. The first is to try to solve the TDSE numerically³, while the second is to seek a way of calculating the transition amplitudes without actually solving the time-dependent Schrödinger equation. We will consider the

³See the outlook

second way. The SFA gives a very simple and physical transparent way of doing this calculation. It consist of neglecting the binding potentials influence on the continuum states, thus using Volkov states instead of the full continuums solutions to (1.9). This assumption is legitimate, provided that the field-strength is large enough to dominate the Coulomb term at the distances where ionization occurs. The long range of the Coulomb potential, however, makes it a bit problematic, especially in the case of a linearly polarized laser pulse [23, 24, 25]. We will return to this point later, where we will consider improvements to this part of the SFA. In addition to the above approximation, we furthermore assume that intermediate resonances do not play a role, which means that we can neglect all bound states, except the ground state. This is again only legitimate, if the field is very strong. S-matrix formalism [20] gives the following expression for the transition amplitude ($i \rightarrow f$), if we employ these assumptions.

$$S_{fi} = \delta_{fi} - i \int_{-\infty}^{\infty} \langle \Psi_{\vec{q}}(\vec{r}, t) | V(t) | \Psi_0(\vec{r}, t) \rangle dt - \sum_{\vec{p}} \int_{-\infty}^{\infty} \int_{-\infty}^{\infty} \theta(t_2 - t_1) \times \langle \Psi_{\vec{q}}(\vec{r}, t_2) | V_B | \Psi_{\vec{p}}(\vec{r}, t_2) \rangle \langle \Psi_{\vec{p}}(\vec{r}, t_1) | V(t_1) | \Psi_0(\vec{r}, t_1) \rangle dt_1 dt_2 + \text{higher order terms} \quad (1.10)$$

Here $\Psi_{\vec{q}}$ is a Volkov-state with asymptotic momentum \vec{q} , Ψ_0 is the ground state, and V_B is the binding-potential. The first term (besides the Kronecker delta) describes direct ionization, while the second term describes ionization followed by rescattering. Higher order terms could, for instance, be ionization followed by recombination, and then finally ionization. We are only interested in direct ionization, so we are going to focus on the first term. Let's assume that the laser-pulse with duration τ starts interacting with the target at $t = 0$.

$$S_{fi} = -i \int_0^{\tau} \langle \Psi_{\vec{q}}(\vec{r}, t) | V(t) | \Psi_0(\vec{r}, t) \rangle dt \quad (1.11)$$

This is our final formula for the transition amplitude, once S_{fi} is known it is straightforward to calculate for example the momentum distribution $\frac{dP_{fi}}{dq_x dq_y dq_z} = |S_{fi}|^2$, which contains the most specific information regarding the ionization process. Whether or not it is possible to calculate S_{fi} in practice, of course depends on the complexity of the matrixelement $\langle \Psi_{\vec{q}}(\vec{r}, t) | V(t) | \Psi_0(\vec{r}, t) \rangle$ i.e., on the complexity of the ground state. The matrixelement is analytical in the case of hydrogen or hydrogen-like atoms, while we have to use the asymptotic (large r) ground state in order to evaluate it analytically in the case of molecules [26]. Another issue regarding molecules is the problem associated with the orientation of the molecule compared to the polarization vector.

Now let us briefly return to the problem regarding the neglect of the Coulomb potential in the final state. The long range of the Coulomb potential makes this assumption problematic, as mentioned earlier. One way to relax this assumption, in the case of hydrogen (or hydrogen like atoms), is to use a so called Coulomb-Volkov wave function instead of the normal Volkov wave function [27].

The Coulomb-Volkov wave function can be thought of as a kind of interpolation between a Coulomb continuum state, i.e., a continuum state for hydrogen, and a Volkov state. It reduces to a Volkov state in the strong-field limit, where $Z \rightarrow 0^4$, and to a continuum state for hydrogen in the weak field limit $E = 0$. Expressed mathematically,

$$\Psi_{CV}(\vec{r}, t) = \Psi_H(\vec{r}, t)L(\vec{r}, t) \quad (1.12)$$

where $\Psi_H(\vec{r}, t)$ is an ingoing Coulomb continuum state [11], and L is the field-dependent part of the Volkov state. The Coulomb-Volkov modified SFA takes the Coulomb-potential into some consideration, but it is important to remember that it is still an approximation. We will mostly use the normal SFA in this report.

1.4 The saddle-point method

Our task within the SFA is, as shown in the previous section, to calculate the integral $\int_0^\tau \langle \Psi_{\vec{q}}(\vec{r}, t) | V(t) | \Psi_0(\vec{r}, t) \rangle dt$. Once this integral is calculated, all physical relevant quantities regarding the ionization process can in principle be found.

This integral is, however, quite difficult to calculate numerically⁵. The matrix-element contains the factor $\exp(iS(t))$, where $S(t) = \frac{1}{2} \int_0^t (\vec{q} + \vec{A})^2 dt' + I_p t$ is the classical action. This makes the integrand oscillate very rapidly. Thus, we need a large number of quadrature points in order to evaluate the integral, making the integration somewhat time consuming.

The saddle-point method (SPM) is a computational convenient way of calculating an approximation to the integral based mathematically on an asymptotic expansion. In addition SPM also gives a large amount of physical insight, since it provides us with a time-analysis of the obtained results.

Imagine that we have to calculate the integral [28],

$$I(\lambda) = \int_C \exp(\lambda f(z)) dz \quad (1.13)$$

where $\lambda \in \mathbb{R}$ is large and C is some contour in the complex plane. Cauchy's theorem tells us that we can deform C as we wish without changing the integral as long as we do not change the end points, which we assume not to contribute to the integral. Now write $f(z) = u(z) + iv(z)$, where u and v is the real and imaginary part of f respectively. The absolute value of the integrand will vary rapidly due to the $\exp(\lambda u)$ part, while the $\exp(i\lambda v)$ part causes the integrand to oscillate rapidly. All of this makes a numerical evaluation hard. The trick is to modify C in such a way that u will climb to a maximum z_0 along C and then quickly fall off, while v stays constant killing the oscillations. Our integral will be dominated by the behavior around z_0 , if such a modification is possible. The first requirement forces the contour to go through a point z_0 where $\nabla u(z_0) = 0$, and Cauchy-Riemanns

⁴ Z is the charge of the residual ion.

⁵It is not possible to evaluate the integral analytically.

theorem then immediately tells us that $\nabla v(z_0) = 0$, hence C has to pass through a saddle-point for f . We proceed by expanding f in a Taylor series to second order around z_0 , remembering that the integral is dominated by z_0 .

$$f(z) \approx f(z_0) + \frac{1}{2} \frac{d^2 f}{dz^2}(z_0)(z - z_0)^2 \quad (1.14)$$

Now defining α , θ , and ρ by setting $z - z_0 = \rho \exp(i\theta)$ and $\frac{d^2 f}{dz^2}(z_0) = \left| \frac{d^2 f}{dz^2}(z_0) \right| \exp(i\alpha)$, then,

$$\frac{1}{2} \frac{d^2 f}{dz^2}(z_0)(z - z_0)^2 = \frac{1}{2} \left| \frac{d^2 f}{dz^2}(z_0) \right| \rho^2 \exp(i(\alpha + 2\theta)) \quad (1.15)$$

Here comes the essential part, if we now choose C in such a way that the angle θ satisfies the relation $\exp(i(\alpha + 2\theta)) = -1$ and keep it fixed varying ρ only ($dz = \exp(i\theta)d\rho$), the integral transforms to,

$$I(\lambda) = \exp(\lambda f(z_0)) \exp(i\theta) \int_{-\infty}^{\infty} \exp\left(-\lambda \left| \frac{d^2 f}{dz^2}(z_0) \right| \frac{\rho^2}{2}\right) d\rho \quad (1.16)$$

which is easily evaluated to $I = \exp(\lambda f(z_0)) \exp(i\theta) \left(\frac{2\pi}{\lambda \left| \frac{d^2 f}{dz^2}(z_0) \right|} \right)^{\frac{1}{2}}$. This formula gives the contribution to the integral from the saddle-point z_0 , which is expected to be the dominant part. In the case of several saddle-points, the integral will be a sum over the contributions from each saddle-point.

Having presented the basic mathematical principles it is time for an example. Consider a hydrogen atom interacting with a few-cycle laser pulse described by (1.8). Straightforward calculations give the following expression for the transition amplitude [22],

$$S_{fi} = \frac{\sqrt{2}}{\pi} \left(\frac{i}{2} \int_0^\tau \frac{1}{S'} \exp(iS) dt - \frac{\exp(iS)}{2S'^2} \right) \quad (1.17)$$

Our goal is to solve the integral $I_{fi} = \frac{i}{2} \int_0^\tau \frac{1}{S'} \exp(iS) dt$ using the SPM. The integral is dominated by the saddle points i.e., the solutions to $S'(t) = 0^6$, and possible by the end points. It turns out that the end points cancel out the $\frac{\exp(iS)}{2S'^2}$ term, and we get $S_{fi} \approx \frac{\sqrt{2}}{\pi} \sum_s I_{fi}^s$ where the sum is taken over the different saddle-points. Notice, however, that the integrand $\frac{1}{S'} \exp(iS)$ is singular at the saddle-point t_s ($S'(t_s) = 0$). This seems to make the SPM inapplicable, but as it turns we only need to modified the SPM slightly [22]. The idea is to shift C slightly below the relevant saddle-point, carry out the same calculations as before and finally letting the shift approach zero. We will not go through the calculations, but only state the final result [22],

$$S_{fi} = -\frac{\sqrt{2}}{2} \sum_s \frac{\exp(iS(t_s))}{S''(t_s)} \quad (1.18)$$

⁶We choose only to consider saddle-points with $0 \leq \text{Re}(t_s) \leq \tau$ and $\text{Im}(t_s) \geq 0$

This formula applies only for hydrogen or hydrogenlike atoms, but the SPM is also applicable for more complex systems, e.g., molecules [26]. The SPM reduces the transition amplitude, which is a complicated integral, to a sum of analytically known terms. It is almost to good too be true and in some sense it is. The saddle-point equation $\frac{1}{2}(\vec{q} + \vec{A})^2 + I_p = 0$ is easy to solve in the monochromatic case, but quite difficult to solve in the few-cycle case. It is impossible to find analytical solutions, so the only way is to find the solutions numerically. This turns out to be relatively time consuming, even through we actually know the number of acceptable solutions⁷. The SPM, however, still contains a great deal of physical insight. The rest of this section is devoted to the physical content.

Consider the following semi-classical model for the ionization process [29]. First the electron is ionized at a specific time $t = t_0$ with initial momentum $\vec{q}(t_0) = 0$. Second it moves like a classical particle under the influence of the laser field only, the Coulomb interaction being neglected. Newton's second law then tells us that, $\frac{d\vec{q}}{dt} = -\vec{E}(t)$. This differential equation has that solution $\vec{q}(t) = \vec{A}(t) - \vec{A}(t_0)$, fulfilling the condition $\vec{q}(t_0) = 0$. The final momentum is,

$$\vec{q}_{\text{final}} = -\vec{A}(t_0) \tag{1.19}$$

since the vector potential is zero after the pulse. Classical mechanics predict that the final momentum is determined by the vector-potential at the time of ionization. Formula (1.19) is incredibly useful when it comes to the interpretation of numerical results and we will use it several times in this report.

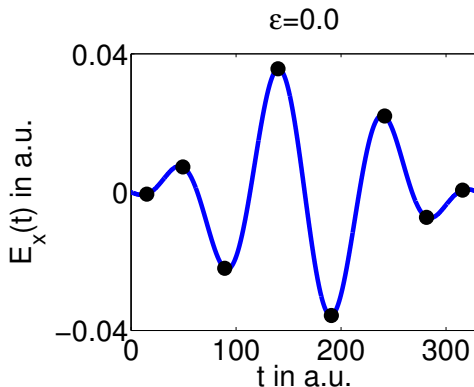


Figure 1.2: The full curve shows the electric field in the case of a linearly polarized field $\epsilon = 0$, with the parameters $I = 5.0 \times 10^{13} \text{ W/cm}^2$, $\phi = 0$, $\omega = 0.057$ corresponding to a central wavelength of 800nm, and $N = 3$. The dots show $E_x(\text{Re}(t_s))$, where t_s are a solution to the saddle-point equation for $\vec{q} = (0.05, 0, 0)$. It is easily checked that $|\text{Re}(A_x(t_s)) - q_x| < 10^{-8}$ for all t_s .

The saddle-point is, as mentioned before, solutions to the equation $\frac{1}{2}(\vec{q} + \vec{A})^2 +$

⁷There are $N + 1$ solutions for a given momentum in the circular case, and $2(N + 1)$ in the linear case [22]

$I_p = 0$. In the strong-field limit where we can neglect the ionization potential I_p , this equation becomes $\vec{q} = -\vec{A}(t_s)$. But that is precisely the classical equation from the semi-classical model. So, the saddle-points can be interpreted as real ionization times in the strong-field limit. In the general case, we cannot neglect the ionization potential and the saddle-points get complex, reflecting the fact that the electron has to go through a barrier. The real part, however, can still be interpreted as a real ionization time since $\vec{q} \approx -\vec{A}(Re(t_s))$ (see fig. 1.2). So the SPM identifies the instants of time which dominates the ionization process, and gives the contribution from each of these. Following Feynman [12], the exact probability amplitude can be written as a path integral $\int D \exp(iS(t))$ where we integrate over all paths leading to direct ionization. This integral reduces to a sum over a finite number of paths, if the process is dominated by these paths, and the SPM, can in some sense, be viewed as a mathematical method for finding these contributions [30].

Chapter 2

Numerical and analytical results

Having presented the general theory, we are now ready to look at some of the results obtained during my Part A. This chapter is based mainly on [1, 2, 3, 4].

2.1 Symmetry of carrier-envelope phase difference effects

In this section (based mainly on [1]), we present a complete characterization of the response of atomic and molecular systems under a change of the carrier-envelope phase difference CEPD. The findings are exemplified by calculation performed on hydrogen using the SFA. We start out by considering an n -electron atom interacting with a few-cycle circularly polarized laser pulse described by the vector potential,

$$\begin{aligned} \vec{A}(\phi, t, \vec{r}) &= \frac{A_0}{\sqrt{2}} f(\eta) \\ &\times (\cos(\eta + \phi) \vec{e}_x + \sin(\eta + \phi) \vec{e}_y) \end{aligned} \quad (2.1)$$

with $f(\eta) = \sin^2(\frac{\eta}{2N})$ being the envelope, N the number of optical cycles, $\eta = \omega t - kz$, ω the frequency, and $\vec{k} = k\vec{e}_z$ the wave vector. Notice that we do not employ the dipole approximation. In this case the time-dependent Schrödinger equation reads,

$$i \frac{\partial}{\partial t} \Psi = \left(H_0 + \sum_{j=1}^n \vec{A}(\phi, t, \vec{r}_j) \cdot \hat{p}_j + \frac{nA_0^2}{4} f^2(\eta) \right) \Psi \quad (2.2)$$

We are interested in relating this equation to an equation for the $\phi = 0$ case. To this end, we note that the z component of the total angular momentum J_z generates rotations around the z axis, implying that the unitary operator $D(\phi) = \exp(iJ_z\phi)$ corresponds to a rotation of our system by an angle $-\phi$ around the z -axis [12]. Since H_0 is invariant under rotations around the z -axis ($[H_0, J_z] = 0$),

the transformed wave function $\Psi' = D(\phi)\Psi$ satisfies the Schrödinger equation

$$i\frac{\partial}{\partial t}\Psi' = (H_0 + \sum_{j=1}^n D(\phi)\vec{A}(\phi, t, \vec{r}_j) \cdot \hat{p}_j D^\dagger(\phi) + \frac{nA_0^2}{4}D(\phi)f^2(\eta)D^\dagger(\phi))\Psi', \quad (2.3)$$

and using the Baker-Hausdorff lemma [12],

$$\exp(iG\lambda)A \exp(-iG\lambda) = A + i\lambda[G, A] + \frac{i^2\lambda^2}{2!}[G, [G, A]] + \dots \quad (2.4)$$

we obtain after some algebra,

$$i\frac{\partial}{\partial t}\Psi' = \left(H_0 + \sum_{j=1}^n \vec{A}(0, t, \vec{r}_j) \cdot \hat{p}_j + \frac{nA_0^2}{4}f^2(\eta) \right) \Psi'. \quad (2.5)$$

When we compare (2.2) and (2.5), we see that a change in the CEPD from $\phi = 0$ to $\phi = \phi'$ corresponds to a rotation of our system around the z -axis by the angle ϕ' . In the above derivation it is essential that the field-free Hamiltonian H_0 is invariant to rotations around the z -axis. If this is not the case, our proof breaks down. As an example we look at ionization of a linear molecule, in a circularly polarized few-cycle laser pulse. If the molecule is aligned along the laser propagation direction, the field-free Hamiltonian still has the required symmetry and the statement holds. We have thus proven the following theorem:

Consider an atomic or molecular system interacting with a circularly polarized few-cycle laser pulse. If the field-free Hamiltonian is invariant under rotations around the propagation direction of the few-cycle pulse a change $\Delta\phi$ in CEPD corresponds to an overall rotation of the total system around the propagation direction by $\Delta\phi$.

By exploiting the invariance of the dot-product under rotations ($\vec{E}(\phi) \cdot \vec{r} = [R_z(\phi)\vec{E}(\phi = 0)] \cdot [R_z(\phi)R_z(-\phi)\vec{r}] = \vec{E}(\phi = 0) \cdot \vec{r}'$, where $R_z(\phi)$ is the 3×3 matrix describing rotations around the z axis), the SFA is readily shown to respond to CEPD changes like the exact theory discussed above. Thus, the theorem also holds in the SFA.

If the molecule is not aligned along this axis, the system does not have the required symmetry and CEPD effects can not be reduced to a geometrical rotation. Accordingly, we may make a distinction between rotational invariant atomic and molecular systems where the CEPD effects are purely geometric rotations, and systems which are not rotational invariant in which case true *non-geometrical* CEPD effects occur. For example, the results on strong-field ionization of K_2^+ with the molecule in the polarization plane [31] belong to the latter category.

The theorem is not only theoretically interesting, but also helpful in practical calculations since this symmetry property reduces the number of computations one has to perform to a single one – all other results are obtained by suitable rotations. For instance, imagine we are interested in the differential ionization probability

$\frac{dP_{fi}}{dq_x dq_y}(\phi)$ for the momenta q_x, q_y in the polarization plane and for a general $\phi > 0$. Then we calculate $\frac{dP_{fi}}{dq_x dq_y}(\phi = 0)$, and rotate the result counterclockwise by an angle ϕ to obtain $\frac{dP_{fi}}{dq_x dq_y}(\phi)$. This is very helpful, since the actual calculation of $\frac{dP_{fi}}{dq_x dq_y}(\phi)$ typically is quite time consuming.

As an illustration, we consider ionization of atomic hydrogen H(1s) in the SFA. Once S_{fi} is known, a simple numerical integration over q_z gives us the (q_x, q_y) distribution $\frac{dP_{fi}}{dq_x dq_y} = \int_{-\infty}^{\infty} |S_{fi}|^2 dq_z$. The time integral in S_{fi} is calculated numerically using Gauss-Legendre quadrature [32], while the integral over q_z is calculated using an equidistant grid on the interval $[-Q_z, Q_z]$, where Q_z is chosen large enough to ensure convergence. All SFA results in this report are calculated in this manner. Figure 2.1 presents the calculated distribution for various values of ϕ . For varying

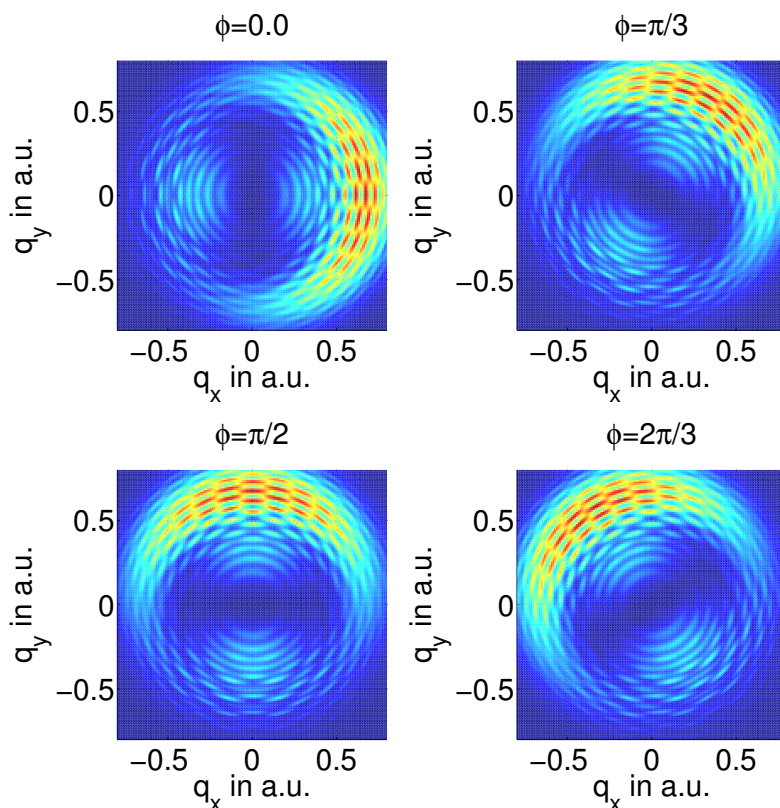


Figure 2.1: The (q_x, q_y) distribution for strong-field ionization of H(1s) for various values of ϕ , with $I = 5.0 \times 10^{13}$ W/cm², $\omega = 0.057$ corresponding to a central wavelength of 800nm and three cycles, $N = 3$. The grid size is $\Delta q_x = \Delta q_y = 0.01$.

ϕ , the distribution rotates in accordance with the general theory. We will return to an examination of these distributions in the subsequent section.

The physics behind all of this, is of course that the field itself rotates when we change CEPD (see fig. 1.1). It is exactly this behavior that allows us to transform (2.2) to (2.5).

Finally let us look a bit on the general case, i.e., the case of a general polarized laser pulse. It is clear that the theorem does not hold for $\epsilon \neq \frac{\pi}{2}$, since the field itself does not have the required symmetry. As shown by Roudnev and Esry, however, it is still possible to find an unitary operator relating $\Psi(\phi = 0)$ to $\Psi(\phi \neq 0)$ [33], but it does not have the nice geometrical meaning as the $\epsilon = \frac{\pi}{2}$ case. CEPD effects are in general caused by interferences between different n-photon channels [33].

2.2 Momentum distributions

Having characterized the response of atomic and molecular systems under a change of the CEPD, let us move on to a detailed investigation on how the ionization process for atoms and molecules depends on the polarization and the pulse length. More precisely we will investigate ionization of hydrogen by a few-cycle laser pulse. The consideration of hydrogen is not a restriction, since we are going to investigate effects characteristic of the pulse and not the particular atomic or molecular system. The most specific information regarding the ionization process is contained in the momentum distribution $\frac{dP_{fi}}{dq_x dq_y dq_z} = |S_{fi}|^2$, i.e., the fully differential ionization probability. Our field, however, does not have a z -component, so it is more appropriate to look at the (q_x, q_y) momentum distribution $\frac{dP_{fi}}{dq_x dq_y} = \int_0^\infty |S_{fi}|^2 dq_z$. We will start by investigating the circular ($\epsilon = \frac{\pi}{2}$) case, returning to the general case later on.

2.2.1 The circular case

Figure 2.2 presents calculated momentum distributions for different values of N , with $I = 5.0 \times 10^{13}$ W/cm², $\omega_0 = 0.057$ (800 nm) and, $\phi = \frac{\pi}{2}$. The panels in the left column show the SFA results obtained with the Volkov wave used as the final state, and the panels to the right show the SFA results obtained with the Coulomb-Volkov wave for the final state. For $N \lesssim 5$ we observe (i) a pronounced asymmetry in the momentum distribution and (ii) a very complicated interference pattern.

As N increases, we observe in fig. 2.2 the gradual emergence of well-resolved circular peaks separated by one photon energy ω . This phenomenon (called above-threshold ionization), where the ejected electron absorbs additional photons in the continuum, is a well known effect in strong monochromatic fields [34]. Very short pulses contain a large number of different frequencies, contributing with almost equal magnitude. This makes the photon picture somewhat more difficult to work with, in the short pulse regime.

2.2.1.1 Asymmetry in the momentum distribution

The dominant direction of electron emission is determined by the CEPD, and the asymmetry is explained by the semi-classical model presented in Sec. 1.4. The direction of ejection is opposite the direction of the vector potential evaluated at

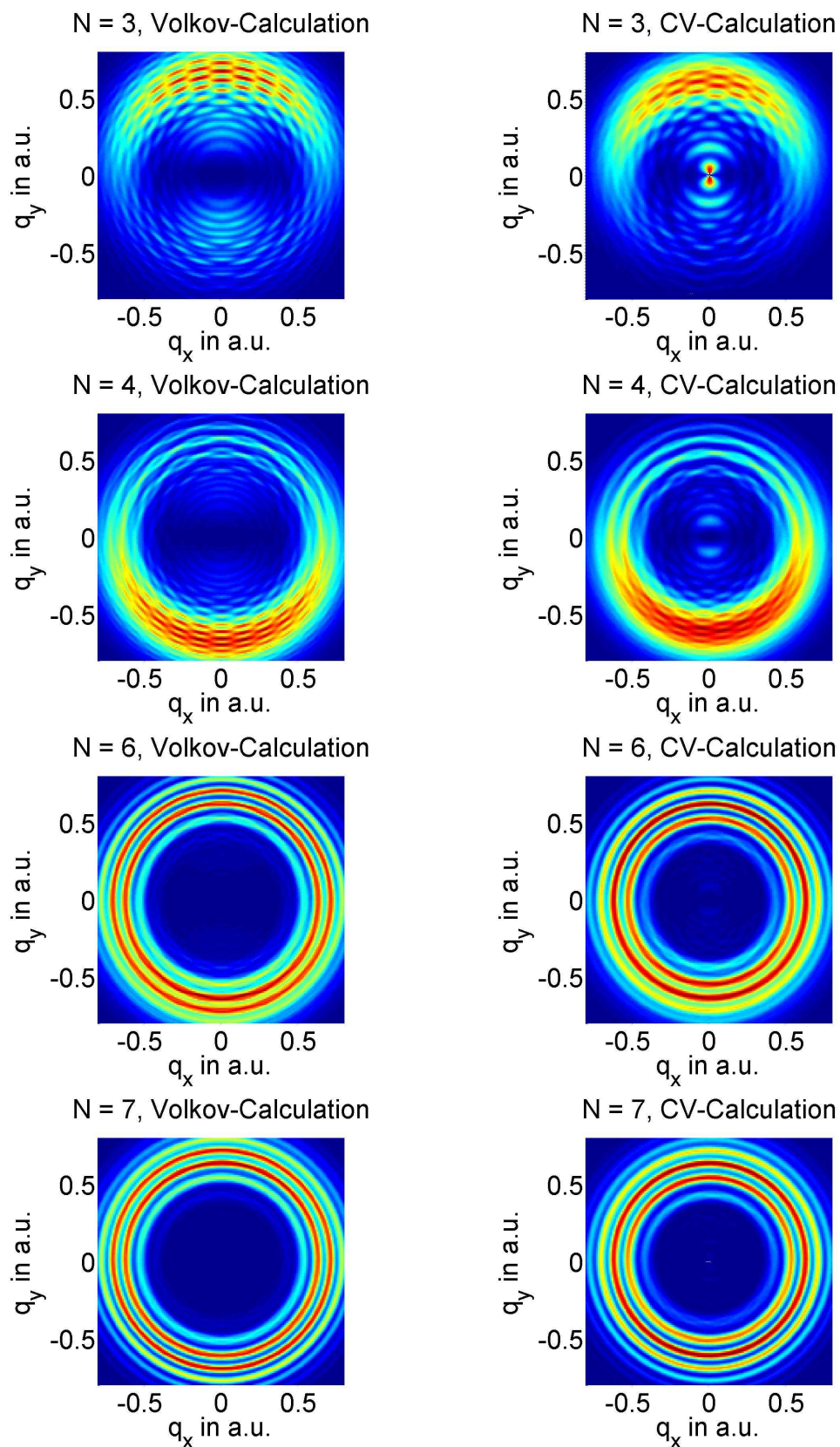


Figure 2.2: Momentum distribution (q_x, q_y) , in the plane of polarization of the right-hand circularly polarized field \vec{E} propagating in the z -direction, for strong-field ionization of H(1s) for various values of N , with $I = 5.0 \times 10^{13} \text{ W/cm}^2$, $\omega_0 = 0.057$ (800 nm), and $\phi = \frac{\pi}{2}$. The grid size is $\Delta q_x = \Delta q_y = 0.01$.

the ionization time. Figure 2.3 shows the vector potential and the corresponding electric field for 3 different values of N . Ionization happens primarily at the instants of time $t_0 = \frac{\tau}{2}$ where the electric field is maximum. Thus, the semiclassical model predicts the following formula $\vec{q} = -\vec{A}(\tau/2)$ for the dominant direction of electron ejection. We observe a good agreement between this simple model and the quantum results in fig. 2.2 for small N . The lack of asymmetry for large N may again be understood in terms of our simple model. For example for $N = 7$, the field takes almost a full revolution on the circle, corresponding to a monochromatic field with our field strength, and t_0 cannot be clearly defined. The signal from a monochromatic field is, of course, symmetric in agreement fig. 2.2.

2.2.1.2 Comparing Volkov and Coulomb-Volkov results

Now we turn to a comparison of the SFA results obtained with the Volkov and the Coulomb-Volkov wave function, respectively. From fig. 2.2 we see that the radial and angular structures are quite similar. There are, however, interesting differences. First, we notice that the distribution obtained with the Coulomb-Volkov wave is shifted slightly towards the origin compared with the Volkov result, and that the distribution is a bit narrower in the former case. This can be explained by the fact that the Coulomb-Volkov wave function takes the attractive Coulomb potential into some consideration. Second, we notice that the SFA calculation with the Coulomb-Volkov wave function reveals some structure in the center for $N = 3$. This is in agreement with the findings in Ref. [24], and can also be explained by the attractive nature of the Coulomb potential. In the classical model this contribution comes from electrons born relatively late (or relatively early) during the pulse, but this model is not appropriate to describe this structure, since it completely neglects the Coulomb potential.

2.2.2 General Polarization

Figure 2.4 presents the calculated momentum distribution for 3 different polarizations $\epsilon = 0, \frac{\pi}{4}, \frac{\pi}{2}$ with $N = 3$, $I = 5.0 \times 10^{13} \text{ W/cm}^2$, $\omega_0 = 0.057$ (800 nm) and, $\phi = 0$. The overall angular structure is again explained by the semi-classical model, reflecting its almost universal validity in explaining strong-field phenomena.

As ϵ is decrease, the distribution gets more narrow and the interference pattern observed in the circular case gradually disappears. In the linear case, we observe a very narrow distribution (compared to the circular case) without any interference pattern. This indicates that subsequent manipulating and steering of the electron is possible only when the field is linear.

2.2.2.1 Comparing SFA and SPM results

It is very instructive to compare the results obtained by a standard SFA calculation with the results obtained from the SPM. The physics behind the interference structure shown in fig. 2.2 are revealed by such a comparison.

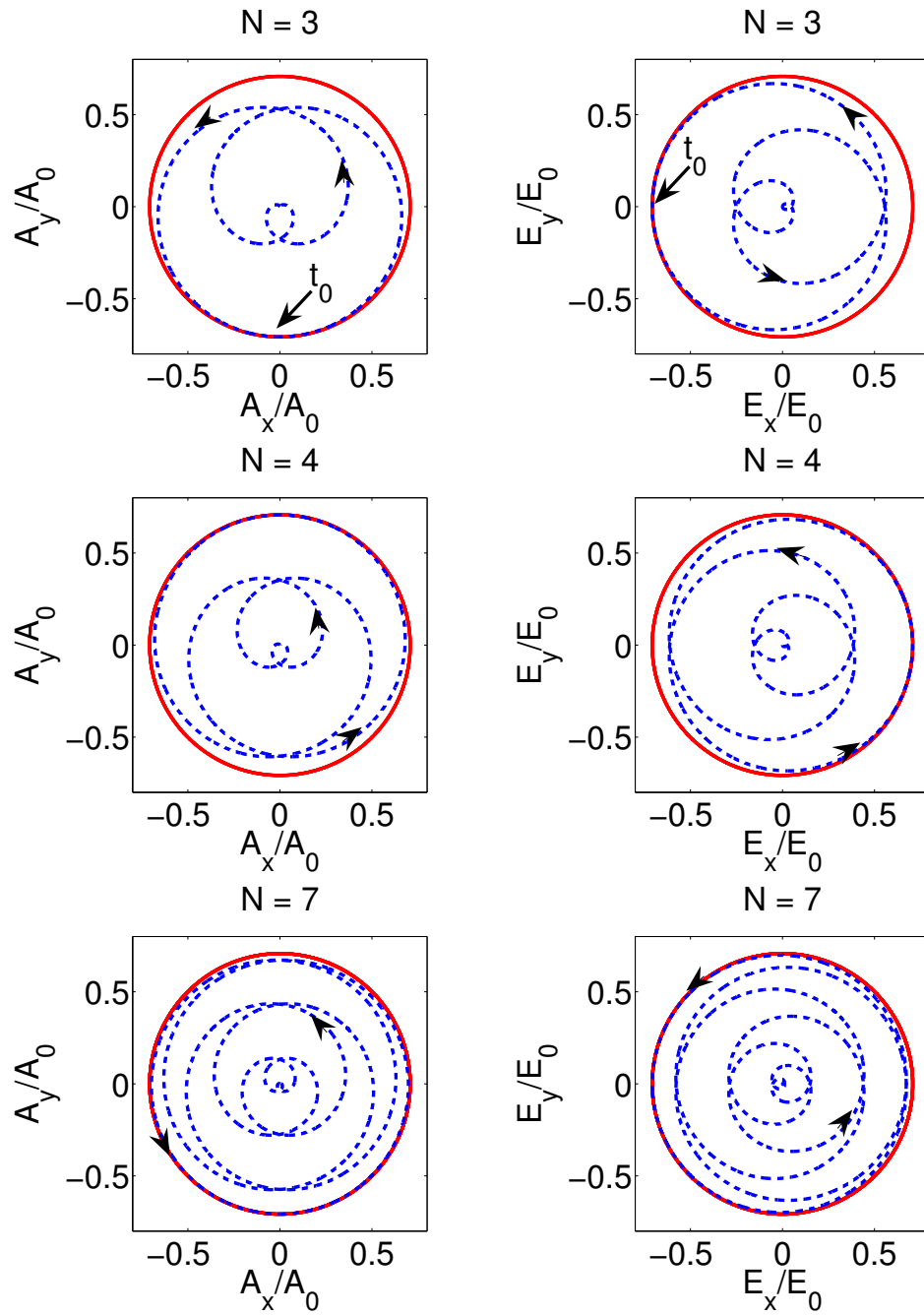


Figure 2.3: Vector potential and electric field (blue dotted line) for 3 different values of N . The solid curve shows the carrier wave, i.e., the field without the envelope. The arrows show the natural time evolution for the pulse. The parameters are $I = 5.0 \times 10^{13} \text{ W/cm}^2$, $\omega_0 = 0.057$ (800 nm), and $\phi = \frac{\pi}{2}$.

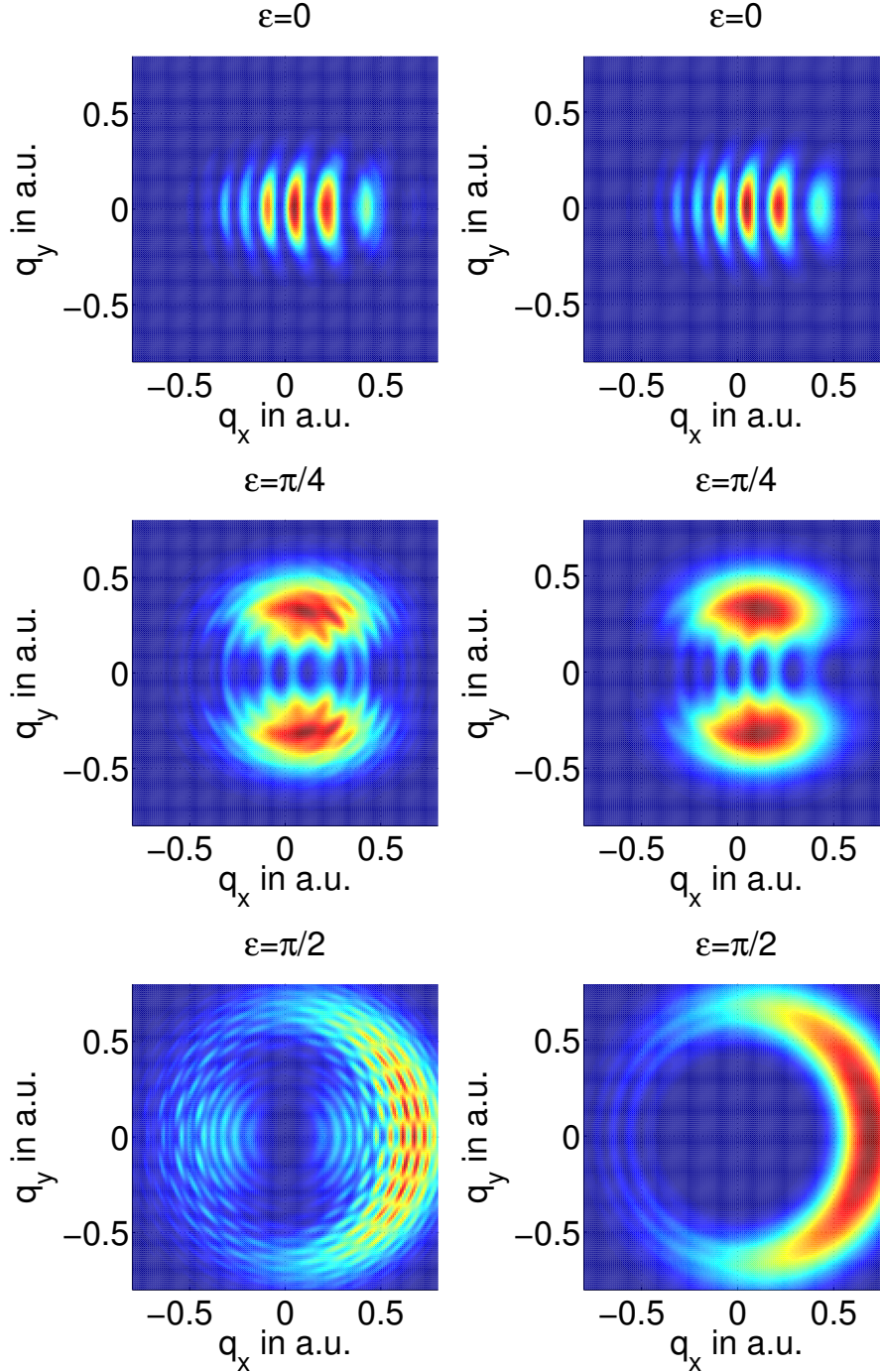


Figure 2.4: Momentum distribution (q_x, q_y) , in the plane of polarization of the right-hand field \vec{E} propagating in the z -direction, for strong-field ionization of H(1s) for various values of ϵ , with $I = 5.0 \times 10^{13} \text{ W/cm}^2$, $\omega_0 = 0.057$ (800 nm), $N = 3$ and $\phi = 0$. The right panels show results obtained from the SFA with the SPM, while the left panels show results obtained from the SFA. The grid size is $\Delta q_x = \Delta q_y = 0.01$.

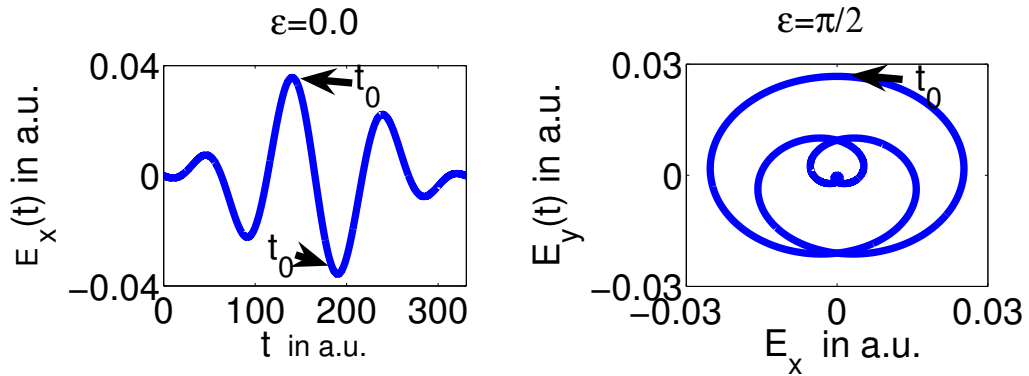


Figure 2.5: The electric field obtained from (1.8) for two different polarizations. The left insert shows the electric field in the case of linear polarization for $\phi = 0$. The right insert shows the electric field in the case of circular polarization for $\phi = 0$ (left). The arrows indicate where the field strength is maximum. The parameters are $I = 5.0 \times 10^{13} \text{ W/cm}^2$, $\omega = 0.057$ corresponding to a central wavelength of 800nm and three cycles, $N = 3$.

Results obtained using the SPM is shown in fig. 2.4. The saddle-point equation was solved numerically using a modified Newton-Raphson method [32].

SPM and SFA yield practical identical results in the case of a linearly polarized pulse, while we observe server discrepancies in the general case, especially in the circular case. As ϵ is increased towards $\epsilon = \frac{\pi}{2}$ an interference pattern emerges in agreement with fig. 2.2. This interference effect is completely absent in the SPM results, the SPM only reproduces the overall structure. The discrepancies between SFA and SPM are explained by the semi-classical model. Differentiating equation 1.19 with respect to t_0 gives,

$$d\vec{q}_{\text{final}} = \vec{E}(t_0)dt_0 \quad (2.6)$$

using $\vec{E} = -\frac{\partial}{\partial t}\vec{A}$. Hence, the spread in momentum $|d\vec{q}|$ is proportional to the spread in ionization time and the ratio is the electric field evaluated at $t = t_0$. A spread in ionization time equal to zero, means that the electron is forced to enter the continuum at $t = t_0$ in order to achieve a final momentum in $(\vec{q}, \vec{q} + d\vec{q})$. Only one path is possible in this case. On the contrary, if $dt_0 > 0$, we have a continuum of paths. Let us restrict ourselves to the region in (q_x, q_y) momentum space with highest yield, in other words the electrons born in the continuum at times near field maximum. The ionization time t_0 , then corresponds to the temporal locations of the global field maxima as illustrated in fig. 2.5.

Figure 2.6 shows $\frac{\max(|\vec{E}|(\epsilon))}{\max(|\vec{E}|(\epsilon=0))}$ as a function of ϵ , i.e., the maximum field strength during the pulse as a function of ϵ . We see that the field maximum during the pulses decreases monotonically as ϵ is increasing. The maximum field strength is about 25 percent smaller in the circular case compared to the linear case. Thus, the spread in ionization time increases as a function of ϵ , allowing more paths

to contribute to the ionization process. This conclusion is reinforced by the fact that the width of the field maximum increases with ϵ . All of this makes the SPM inaccurate, since it only accounts for a fixed finite number of paths. In figure 2.4 each pixel represents 4 pairs of momentum, and hence each pixel is calculated using $4(N + 1)$ saddle points in the circular case and $8(N + 1)$ in the linear case. Figure 2.6 also shows that the interferences observed in fig. 2.2 can be explained by interference between ionization pathways leading to the same final state from different instants of time. The interferences, however, cannot be associated with the different t_s 's.

Figure 2.6 indicates that SPM for the circular case should improve if $\max(|\vec{E}|(\epsilon))$ is increased by a factor of roughly 1.35, corresponding to an intensity of roughly $I = 9.0 \times 10^{13} \text{ W/cm}^2$, and fig. 2.7 shows that this is indeed the case. The interference pattern almost disappears in the SFA result, and the agreement between SFA and SPM is quite satisfactory.

The agreement between SPM and SFA also increases when the number of cycles is increased, as shown in fig. 2.8 and fig. 2.2. This feature seems to contradict with the argument based on the semi-classical model, but this is not the case. We obtain an energy conserving delta function in the expression for S_{fi} in the monochromatic limit $N \rightarrow \infty$, since the width in energy decreases as N increases. Thus, no spread in momentum is allowed and the semi-classical argument fails in the limit $N \rightarrow \infty$.

2.3 Angular distributions from laser-aligned CS₂ molecules: Comparing theory with experiment

We start by a very brief review of the experiment reported in [3], performed by our collaborators at Femtolab¹. They used a pump-probe scheme to investigate how ionization of the linear molecule CS₂ depends on the angle α between the internuclear axis and the polarization vector of the linearly (x-axis) polarized ionization pulse. More precisely, they investigate how the photoelectron angular distribution (PAD) from each photon channel² depends on α .

The CS₂ molecules are first aligned along a given direction using a 0.5 ps (FWHM), $I = 2.9 \times 10^{12} \text{ W/cm}^2$ linearly polarized pump pulse. This pulse is too weak to ionize CS₂, so its sole purpose is to align the molecules, i.e., to orient the molecules in a particular direction with respect to the probe pulse polarization vector. The CS₂ molecules are then, after a delay³, exposed to the 25 fs (FWHM), $I = 7.7 \times 10^{13} \text{ W/cm}^2$ ionizing pulse. This pulse is strong enough to eject the single HOMO electron of CS₂. Electrons produced are detected using a velocity map imaging spectrometer and thereby recorded using a CCD camera. Their results

¹Department of Chemistry, University of Aarhus

²The ionizing pulse is quite long, so the photon picture is a good description

³Corresponding to the first half revival.

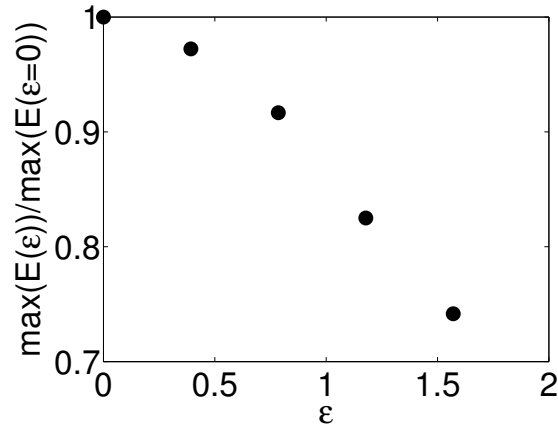


Figure 2.6: The maximum field strength during the pulse as a function of ϵ . The parameters are $I = 5.0 \times 10^{13} \text{ W/cm}^2$, $\omega = 0.057$ corresponding to a central wavelength of 800nm and three cycles, $N = 3$.

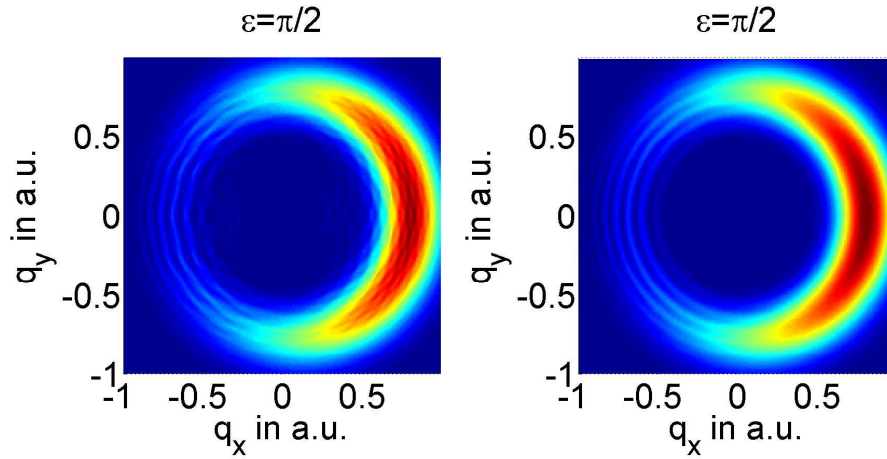


Figure 2.7: Momentum distribution (q_x, q_y) , in the plane of polarization of the right-hand field \vec{E} propagating in the z -direction, for strong-field ionization of H(1s), with $\epsilon = \frac{\pi}{2}$, $I = 9.0 \times 10^{13} \text{ W/cm}^2$, $\omega_0 = 0.057$ (800 nm), $N = 3$ and $\phi = 0$. The right panels show results obtained from the SPM, while the left panels show results obtained from the SFA. The grid size is $\Delta q_x = \Delta q_y = 0.01$.

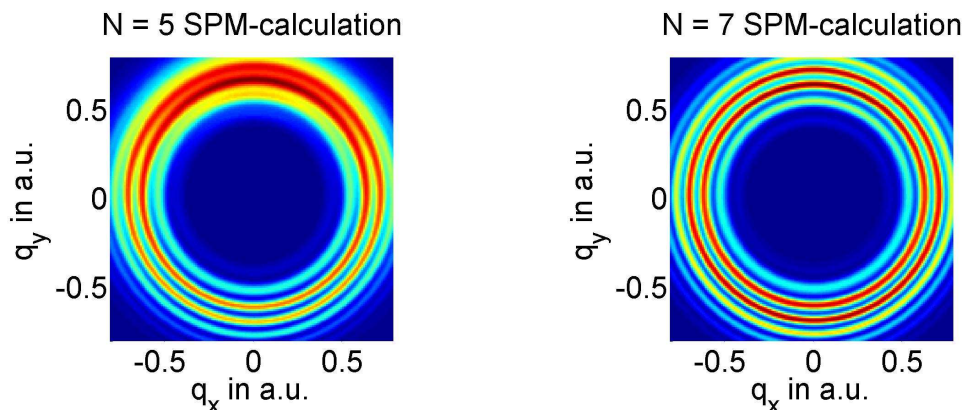


Figure 2.8: SPM momentum distribution (q_x, q_y) , in the plane of polarization of the right-hand field \vec{E} propagating in the z -direction, for strong-field ionization of H(1s), with $\epsilon = \frac{\pi}{2}$, $I = 5.0 \times 10^{13}$ W/cm², $\omega_0 = 0.057$ (800 nm), and $\phi = \frac{\pi}{2}$. The grid size is $\Delta q_x = \Delta q_y = 0.01$.

are shown in fig. 2.9.

Our goal is to model this experiment, using the SFA. In order to do this, we have to take two important things into consideration: laser-volume effects and effects originating from the alignment pulse.

Let us start with laser-volume effects. All the calculations in this report, so far, are performed on a single atom or molecule situated at the center of the laser-beam. In an experiment, however, there are a large number of molecules, and only a fraction of these are situated near the center of the beam, which means that only a fraction of the molecules actually experiences the real peak intensity⁴. The remaining molecules experience a lower max intensity, depending on where they are situated within the beam. We have to make a volume weighted average over all the different intensities, in order to compensate for this effect.

Now what about the alignment part. The alignment pulse creates a coherent superposition of different rotational states, meaning the the orientation of the internuclear axis becomes time-dependent. Shortly after the pump pulse, the molecules are primarily aligned along the polarization axis for the pump pulse. As time goes, the molecules rotate, and after a delay (0.76 ps in our case) the molecules are again primarily align along the polarization axis for the pump pulse. This is the basic principle behind field-free alignment. The degree of alignment is described by the distribution $G_\alpha(\Omega_{\vec{R}})$, where \vec{R} denotes the internuclear axis. We have to average our calculated signal over all the different orientations weighted by the alignment distribution, in order to compare with the experiment.

Now we are ready to go through the procedure. First we calculate the single molecule momentum distribution $\frac{dP}{dq_x dq_y}(q_x, q_z; I, \Omega_{\vec{R}})$ for a number of different intensities I and orientations $\Omega_{\vec{R}}$. This is done using the SFA, and SPM, where we

⁴The intensity at the center of the beam

use the asymptotic ground state wave function for the HOMO of CS₂. We will expect large distances to be the most dominant part of space in ionization, which motivates this approximation. Notice that this conclusion does not hold in velocity gauge, since it probes small distances. The asymptotic ground state has the form,

$$\Phi_0(\vec{r}) = \sum_{lm} C_{lm} r^{\frac{1}{\kappa}-1} \exp(-\kappa r) Y_{lm}(\hat{r}) \quad (2.7)$$

in the body-fixed frame⁵. Here κ is related to the binding energy by $\kappa = \sqrt{2E_b}$. Our asymptotic expansion coefficients C_{lm} are obtained by a Hartree-Fock calculation [26]. We have to express the ground state in the laboratory frame⁶, in order to calculate S_{fi} and hence $\frac{dP}{dq_x dq_y}(q_x, q_z; I, \Omega_{\vec{R}})$. This is done, using Wigner rotation matrices $D(\Omega_{\vec{R}})$ [12]. Having obtained $\frac{dP}{dq_x dq_y}(q_x, q_z; I, \Omega_{\vec{R}})$, we perform the intensity averaging [35] and the average over all the different orientations⁷ to obtain the measurable signal $\left(\frac{dP}{dq_x dq_y}(q_x, q_z)\right)_{\text{experiment}}$. Finally, we integrate radially over each multiphoton peak in order to obtain the PAD for each multiphoton channel. Our results are shown in fig. 2.9. The theoretical results are clearly in qualitative agreement with the experimental results, with minima in the signals at $\phi_{2d} = 90^\circ$ (270°) and maxima around $\phi_{2d} = 0^\circ$ (180°). There are, however, significant discrepancies. Our SFA model generally overestimates the angle dependence, and the order of the curves are wrong. Theory predicts in decreasing order $\alpha = 0^\circ, 45^\circ, \text{unaligned}, 90^\circ$, while the experimental data gives $\alpha = 45^\circ, \text{unaligned}, 0^\circ, 90^\circ$ for the 11 and 12 photon channels, $\alpha = 45^\circ, 0^\circ, \text{unaligned}, 90^\circ$ for the 13 and 14 photon channels. The discrepancies between theory and experiment is probably associated with the excited state spectrum of the CS₂ molecule and the neglect of the final Coulomb interaction. SFA, as mentioned earlier, completely neglects the excited states and the final Coulomb interaction. They actually observed signature of intermediate Rydberg states in the experimental data [3], indicating that excited states do play a role in the experiment.

Another possible source to the discrepancies, is the use of the SAE, but calculations show that the signal from the LUMO is completely suppressed compared to the signal from the HOMO. This is due to the large difference in binding energy ($I_{HOMO} = 10.08\text{eV}$, $I_{LUMO} = 14.60\text{eV}$) between the HOMO and LUMO. A third explanation could be a bending of the linear CS₂ molecule, but as before this is ruled out by calculations. The PAD is not altered significantly if we reduce the S-C-S angle from 180° to 140° (The minimal bending angle possible).

Understanding the PAD for molecules like CS₂ is one of the many challenges to theory in the future.

⁵The frame defined by demanding that the x-axis is the internuclear axis.

⁶The frame defined by demanding that the polarization axis of the ionizing pulse is the x-axis.

⁷This part of the calculation is performed by C. B. Madsen, Department of Physics and Astronomy

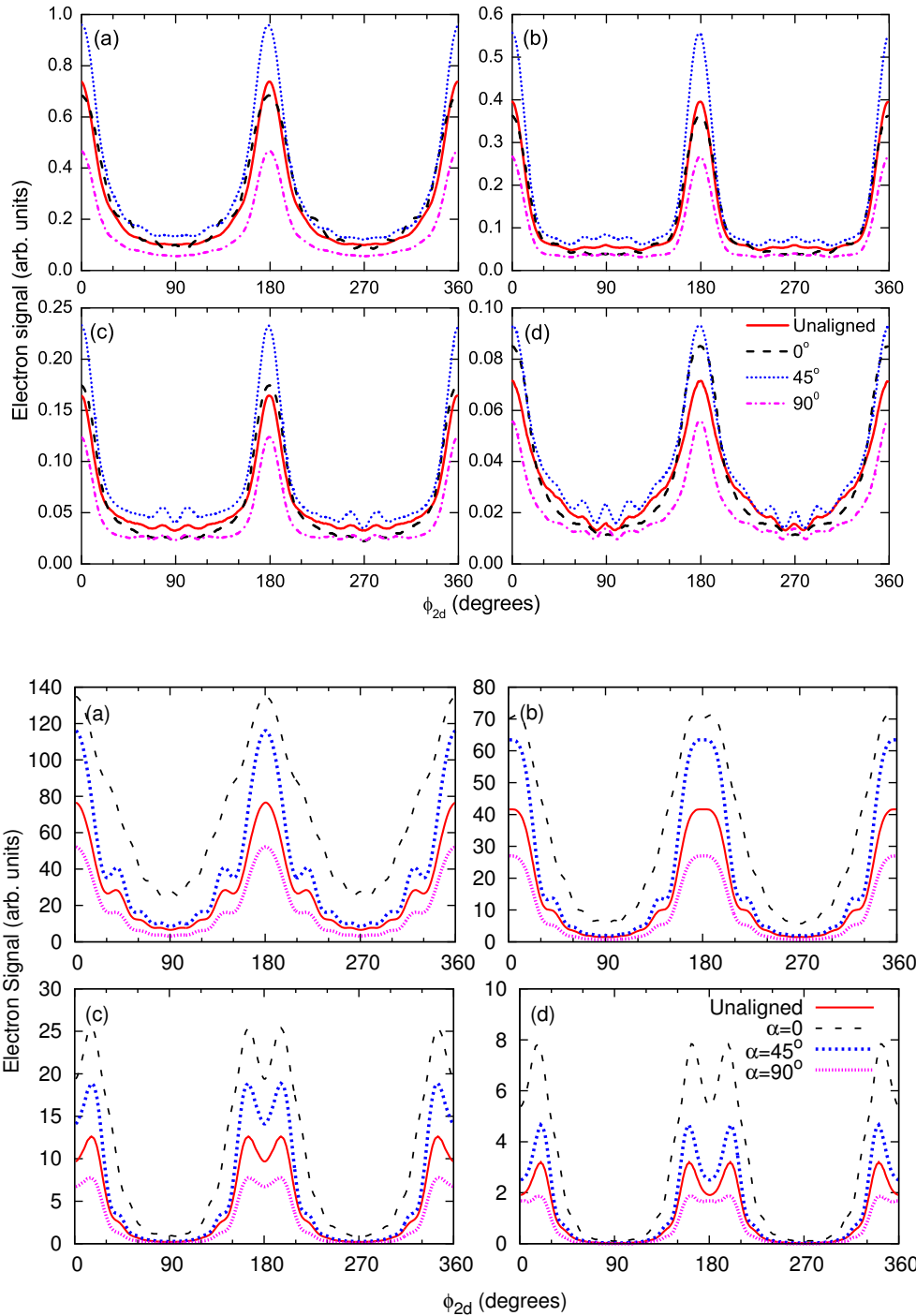


Figure 2.9: PADs for the (a) 11-, (b) 12-, (c) 13- and (d) 14-photon ionization channels. Here ϕ_{2d} , is the angle between the (q_x, q_y) projected electron ejection direction and the x-axis. The upper insert shows the experimental results, while the lower insert shows the theoretical (SFA) predicted PADs

Chapter 3

Conclusion and outlook

3.1 Conclusion

In this report we investigated strong-field few-cycle ionization of atoms and molecules. More precisely, we examined how the ionization process depends on the exact shape (CEPD and the ellipticity of the pulse) of the pulse and the pulse length. Furthermore, we studied how ionization of the linear molecule CS_2 depends on the angle α between the internuclear axis and the polarization vector.

CEPD effects were completely characterized in the circular case, where they just correspond to simple rotations of the total system.

Confinement in the direction of electron ejection and locality in time depends critically on the polarization of the light pulse used and on the pulse length. As an illustration we calculated the momentum distribution for strong-field ionization of hydrogen, using the SFA. The results were compared with results obtained from the SPM, an approximation closely related to the physical interpretation of strong-field ionization. We showed that while the SPM is applicable in the case of linear polarized ionization pulses, it gradually breaks down when the ellipticity is changed towards the circular case. This feature was explained by noting that the maximum field strength during the pulse decreases monotonically as a function of ellipticity, together with the fact that the width of the field maximum increases with ϵ .

Our SFA calculations on CS_2 was in qualitative agreement with the experimental results obtained by our collaborators at Femtolab, but failed at a quantitative level. The discrepancies between theory and experiment may be associated with the excited state spectrum of the CS_2 molecule and the neglect of the final Coulomb interaction.

3.2 Outlook

We plan, in the nearest future, to do ab-initio calculations, i.e., solve the TDSE numerically. A former member of the group, T. K. Kjeldsen has already written a code, based on the split-step method, for solving the SAE TDSE for an atom or

molecule interacting with a linearly polarized laser pulse.

Suppose we know the reduced wave function at some specific instant of time t_0 , and want to calculate it at a later time $t > t_0$. Now,

$$\Phi(\vec{r}, t) = U(t, t_0)\Phi(\vec{r}, t_0) \quad (3.1)$$

where U is the time-evolution operator [12]. The time-evolution operator has the simple form $\exp(-iH(t - t_0))$, if the Hamiltonian is independent of time. Our Hamiltonian, of course, depends on time via the field, and U cannot be written on such a compact form. It is, however, accurate to replace $H(t)$ by the time independent $H((t - t_0)/2)$, provided that $t - t_0$ is small compared to the characteristic timescale for $H(t)$. This means that, $\Phi(\vec{r}, t) \approx \exp(-iH(t - t_0)/2)\Phi(\vec{r}, t_0)$.

The exponential of a operator A , is defined as $\exp(A) = \sum_{n=0}^{\infty} \frac{A^n}{n!}$, making the calculation of $U\Phi$ very difficult in general. If, however, f_a is an eigenfunction for A with eigenvalue a things get easy, since $\exp(A)f_a = \sum_{n=0}^{\infty} \frac{A^n}{n!} f_a = \sum_{n=0}^{\infty} \frac{a^n}{n!} f_a = \exp(a)f_a$. This means that $\exp(A)$ is easier to calculate, if one uses a representation where A is diagonal.

Our Hamiltonian is given by, $H = \left(\frac{1}{2}\frac{\partial^2}{\partial r^2} + \frac{L^2}{2r^2} + V(\vec{r}, t)\right)$, since we are looking at the reduced wave function. We cannot split the operator exponential $\exp(iH(t - t_0))$, due to the fact that we are looking at non-commuting operators. It can be shown, however, that [36]

$$U(t + \Delta t, t) = \exp\left(i\frac{\Delta t}{2}\frac{1}{2}\frac{\partial^2}{\partial r^2}\right) \exp\left(-i\frac{\Delta t}{2}\frac{L^2}{2r^2}\right) \exp(i\Delta t V(\vec{r}, t)) \exp\left(-i\frac{\Delta t}{2}\frac{L^2}{2r^2}\right) \exp\left(i\frac{\Delta t}{2}\frac{1}{2}\frac{\partial^2}{\partial r^2}\right) + O(\Delta t^3) \quad (3.2)$$

The basic idea behind the split-step method is to use this relation, and then represent the wave-function in a representation where the propagating term is diagonal. One obvious task, would be to generalize our present code to general polarization. This would give us the opportunity to test the validity of the results obtained during Part A, and hence test the validity of the SFA, and the SPM. It would also be interesting to test different modifications of the standard SFA like, for instance, Coulomb-Volkov modified SFA.

Next, we plan to study sub-cycle dynamics, i.e., to study the dynamics of the electron during the pulse. Tremendous progress in laser technology has made it possible to investigate ionization dynamics, during the ionizing pulse. M. Uiberacker et. al [37] used a pump-probe experiment to investigate ionization of Ne^+ , during the ionizing few-cycle pulse. They placed Ne in a NIR few-cycle laser-pulse, with an intensity too low to effectively ionize Ne. After a variable delay a 250 attosecond XUV pulse ionized some of Ne population, thus creating positive neon ions in excited states. The binding-energy of these states was 13.6 eV or less, making ionization by the NIR pulse possible. The neon ions are "born" almost instantly, due to short duration of the XUV pulse compared to the NIR pulse. By varying the delay, they scan over the NIR few-cycle pulse, thus allowing them to

investigate ionization of Ne^+ during the ionization process itself.

Until now almost all the theoretical research within the field, has focused on, the question: What happens after the pulse. This experiment opens the door to a whole new branch, where it is relevant to ask what happens during the pulse.

Our SAE TDSE code is a powerful tool for modeling experiments like the above, but the interpretation would benefit highly from a simple model like, for instance, the SFA.

The SFA gives the following expression,

$$P_{\vec{q}}(t) = \left| \int_0^t \langle \Psi_{\vec{q}}(\vec{r}, t) | V(t) | \Psi_0(\vec{r}, t) \rangle dt \right|^2 \quad (3.3)$$

for the probability of being in a Volkov state with asymptotic momentum \vec{q} at time $t < \tau$. Hence,

$$\Gamma_{\vec{q}}(t) = \frac{d}{dt} \left| \int_0^t \langle \Psi_{\vec{q}}(\vec{r}, t) | V(t) | \Psi_0(\vec{r}, t) \rangle dt \right|^2 \quad (3.4)$$

is the rate for ionization with momentum \vec{q} at time t . We already have all the tools for calculating this quantity, and henceforth model sub-cycle dynamics using SFA. We may also use different approach like Coulomb-Volkov SFA, or lowest order perturbation theory within each half cycle.

In the more distant future, we would like to propose different control schemes, based on the obtained knowledge, for electron dynamics in atom and molecules.

Bibliography

- [1] C. P. J. Martiny and L. B. Madsen. **Symmetry of Carrier-Envelope Phase Difference Effects in Strong-Field, Few-Cycle Ionization of Atoms and Molecules.** *Phys. Rev. Lett*, 97:093001, 2006.
- [2] C. P. J. Martiny and L. B. Madsen. **Finite-bandwidth effects in strong-field ionization of atoms by few-cycle circularly polarized laser pulses.** *Phys. Rev. A*, 76:043416, 2007.
- [3] V. Kumarappan, L. Holmegaard, C. Martiny, C. B. Madsen, T. K. Kjeldsen, S. S. Viftrup, L. B. Madsen, and H. Stapelfeldt. **Multiphoton Electron Angular Distributions from Laser-Aligned CS₂ Molecules.** *Phys. Rev. Lett*, 100:093006, 2008.
- [4] C. P. J. Martiny and L. B. Madsen. **Steering an electron wave packet into the continuum.** In preparation, 2008.
- [5] A. Scrinzi, M. Yu. Ivanov, R. Kienberger, and D. M. Villeneuve. **Attosecond physics.** *J. Phys. B*, 39:R1, 2006.
- [6] A. H. Zewail. **Femtochemistry: Atomic-Scale Dynamics of the Chemical Bond.** *J. Phys. Chem. A*, 104:5660, 2000.
- [7] S. Baker, J. S. Robinson, C. A. Haworth, H. Teng, R. A. Smith, C. C. Chirilă, M. Lein, J. W. G. Tisch, and J. P. Marangos. **Probing Proton Dynamics in Molecules on an Attosecond Time Scale.** *Science*, 312:424, 2006.
- [8] J. Itatani, J. Levesque, D. Zeidler, H. Nikura, H. Pépin, J. C. Kieffer, P. B. Corkum, and D. M. Villeneuve. **Tomographic imaging of molecular orbitals.** *Nature*, 432:867, 2004.
- [9] M. F. Kling, Ch. Siedschlag, A. J. Verhoef, J. I. Khan, M. Schultze, Th. Uphues, T. Ni, M. Uiberacker, M. Drescher, F. Krausz, and M. J. J. Vrakking. **Control of Electron Localization in Molecular Dissociation.** *Science*, 312:246, 2006.
- [10] J. D. Jackson. *Classical Electrodynamics.* John Wiley and Sons, 1999.
- [11] B. H. Bransden and C. J. Joachain. *Physics of Atoms and Molecules.* Prentice Hall, 2003.

- [12] J. J. Sakurai. *Modern Quantum Mechanics*. Addison-Wesley Publishing Company, 1994.
- [13] T.K. Kjeldsen and L. B. Madsen. **Strong-field ionization of N₂: length and velocity gauge strong-field approximation and tunneling theory.** *J. Phys. B*, 37:2033, 2004.
- [14] D. Bauer, D. B. Milošević, and W. Becker. **Strong-field approximation for intense-laser-atom processes: The choice of gauge.** *Phys. Rev. A*, 72:023415, 2005.
- [15] D. M. Volkov. **über eine klasse von lösungen der diracschen gleichung.** *Z. Phys*, 94:250, 1935.
- [16] L. B. Madsen. **Strong-field approximation in laser-assisted dynamics.** *Am. J. Phys*, 73:57, 2004.
- [17] L. B. Madsen. *Strong field dynamics: Scattering and Multiphoton ionization*. PhD thesis, University of Aarhus, 1998.
- [18] L. V. Keldysh. **Ionization in the field of a strong electromagnetic wave.** *J. Exp. Theor. Phys*, 47:1945, 1964.
- [19] F. H. M. Faisal. **Multiple absorption of laser photons by atoms.** *J. Phys. B*, 6:L89, 1973.
- [20] H. R. Reiss. **Effect of an intense electromagnetic field on a weakly bound system.** *Phys. Rev. A*, 22:1786, 1980.
- [21] M. Lewenstein, Ph. Balcou, M. Yu. Ivanov, A. L’Huillier, and P. B. Corkum. **Theory of high-harmonic generation by low-frequency laser fields.** *Phys. Rev. A*, 49:2117, 1994.
- [22] D. B. Milošević, G. G. Paulus, D. Bauer, and W. Becker. **Above-threshold ionization by few-cycle pulses.** *J. Phys. B*, 39:R203, 2006.
- [23] D. Arbó, J. E. Miraglia, M. S. Gravielle, K. Schiessl, E. Persson, and J. Burgdörfer. **Coulomb-Volkov approximation for near-threshold ionization by short laser pulses.** *Phys. Rev. A*, 77:013401, 2008.
- [24] A. de Bohan, B. Piraux, L. Ponce, R. Taïeb, V. Vénier, and A. Marquet. **Direct and Indirect Pathways in Strong Field Atomic Ionization Dynamics.** *Phys. Rev. Lett*, 89:113002, 2002.
- [25] O. Smirnova, M. Spanner, and M. Ivanov. **Coulomb and polarization effects in sub-cycle dynamics of strong-field ionization.** *J. Phys. B*, 39:S307, 2006.

- [26] T. K. Kjeldsen and L. B. Madsen. **Strong-field ionization of atoms and molecules: The two-term saddle-point method.** *Phys. Rev. A*, 74:023407, 2006.
- [27] G. Duchateau, E. Cormier, H. Bachau, and R. Gayet. **Coulomb-Volkov approach of atom ionization by intense and ultrashort laser pulses.** *Phys. Rev. A*, 63:053411, 2001.
- [28] M. Yu. Ivanov. **Dealing with complicated integrals: saddle point-type methods and some applications.** 2002.
- [29] S. Chelkowski and A. D. Bandrauk. **Sensitivity of spatial photoelectron distributions to the absolute phase of an ultrashort intense laser pulse.** *Phys. Rev. A*, 65:061802, 2002.
- [30] P. Salières, B. Carré, L. Le Déroff, F. Grasbon, G. G. Paulus, H. Walther, R. Kopold, W. Becker, D. B. Milošević, A. Sanpera, and M. Lewenstein. **Feynman's Path-Integral Approach for Intense-Laser-Atom Interactions.** *Science*, 292:902, 2001.
- [31] S. X. Hu and L. A. Collins. **Strong-field ionization of molecules in circularly polarized few-cycle laser pulses.** *Phys. Rev. A*, 73:023405, 2006.
- [32] W. H. Press, S. A. Teukolsky, W. T. Vetterling, and B. P. Flannery. **Numerical Recipes.** Cambridge University Press, 1992.
- [33] V. Roudnev and B. D. Esry. **General Theory of Carrier-Envelope Phase Effects.** *Phys. Rev. Lett*, 99:220406, 2007.
- [34] P. Agostini, F. Fabre, G. Mainfray, G. Petite, and N. K. Rahman. **Free-Free Transitions Following Six-Photon Ionization of Xenon Atoms.** *Phys. Rev. Lett*, 42:1127, 1979.
- [35] T. Morishita, Z. Chen, S. Watanabe, and C. D. Lin. **Two-dimensional electron momentum spectra of argon ionized by short intense lasers: Comparison of theory with experiment.** *Phys. Rev. A*, 75:023407, 2007.
- [36] T. K. Kjeldsen. **Wave packet dynamics studied by ab initio methods: Applications to strong-field ionization of atoms and molecules.** PhD thesis, University of Aarhus, 2007.
- [37] M. Uiberacker, Th. Uphues, M. Schultze, A. J. Verhoef, V. Yakovlev, M. F. Kling, J. Rauschenberger, N. M. Kabachnik, H. Schröder, M. Lezius, K. L. Kompa, H. G. Muller, M. J. J. Vrakking, S. Hendel, U. Kleineberg, U. Heinzmann, M. Drescher, and F. Krausz. **Attosecond real-time observation of electron tunnelling in atoms.** *Nature*, 446:627, 2007.